Numerical simulation of tornado flows using anisotropic mesh adaptation

Miguel A. Aguirre[1], Renato V. Linn[1], Alexandre L. Braun[1]

[1]*Centro de Mecânica Aplicada e Computacional (CEMACOM)*
Programa de Pós-Graduação em Engenharia Civil (PPGEC)
Universidade Federal do Rio Grande do Sul (UFRGS)
Av. Osvaldo Aranha, 99, 90035-190, Porto Alegre, RS, Brazil
miguel.aguirre@ufrgs.br, renatolinn@ufrgs.br, alexandre.braun@ufrgs.br

Abstract. A numerical model for tornado flow simulation is proposed in this work, where Adaptive Mesh Refinement (AMR) techniques are utilized. Owing to the increase observed in the annual occurrence of storms with tornado formation, investigations on tornado flow characteristics and its effects on buildings and structures are required. In this sense, a numerical algorithm based on the explicit Characteristic-Based Split (CBS) scheme is adopted to solve the system of flow equations, where four-node tetrahedral finite elements are employed in the spatial discretization procedures. An anisotropic mesh adaptation scheme based on Riemannian metric is coupled to the flow solver in order to capture high flow variable gradients in the tornado vortex region. Tornado flow fields are simulated here using numerical modeling of tornado experimental simulators and results obtained with the present model are compared with predictions presented by other authors in order to evaluate the influence of mesh adaptation on the accuracy of the numerical results.

Keywords: Tornado Flows, Adaptive Mesh Refinement (AMR), Finite Element Method (FEM).

1 Introduction

Tornadoes are natural phenomena that occur on all the five continents, although they are more frequent in the central region of the United States, southern Brazil, northern Argentina and in the vicinity of the Himalayas [1]. In the last century, it was believed that tornadoes were quite rare in Brazil because only some events were captured by radar equipments. However, through media coverage and the advent of the Internet, the frequency of reports of these events has increased significantly in recent decades [2].

The action of a tornado is localized and of short duration, which makes it difficult to study real events in detail. Therefore, since the 70's tornado vortex chambers (TVCs) have been developed. In this sense, Ward [3] made a simulator that allowed to analyze the effect of the geometric configuration on the vortex patterns. Also, Haan et al. [4] demonstrated that Iowa State University's translating chamber was able to simulate the flow patterns of real tornadoes. Mishra et al. [5] presented the Texas Technological University simulator and compared the measurements obtained with predictions from analytical and numerical models and two real tornadoes. Refan [6] used flow visualization methods to test tornadoes in the WindEEE dome.

On the other hand, with constant improvements observed in computers technology, numerical simulations have been also adopted. Among the different approaches available, tornado scale models that reproduce the shape of experimental simulators allow the study of flow patterns and their action on buildings with reasonable computational cost. Since the flow field developed during a tornado event is complex, mesh adaptation techniques are required to obtain accuracy and rational use of the finite element mesh. In this context, Nolan et al. [7] used a mesh-adapted numerical model to investigate the influence of domain size and Reynolds number on the numerical predictions. Nolan et al. [8] concluded that the same scheme can reproduce a full resolution model through levels of refinement as a function of the flow. Natarajan [9] utilized Fluent 6.3 to study the flow

characteristics considering the Ward-type Tornado Vortex Chamber (TVC), the WinDEEE Dome and the Atmospheric Vortex Engine (AVE), where mesh adaption was adopted.
In the present work, a numerical model with adaptive mesh is proposed to reproduce the tornado flow field with low Reynolds Number in a Tornado Vortex Chamber. A finite element model based on the explicit CBS scheme is used, where linear tetrahedral elements are adopted for spatial discretization. Mesh adaptation including refinement, coarsening and node movement is performed anisotropically based on a Riemannian metric field for error estimation.

2 Flow fundamental equations and numerical model

A general purpose numerical code developed by Linn [10] is adopted here to simulate the flow field in a tornado vortex chamber. In order to reproduce incompressible flows, boundary conditions and Mach number must be specified accordingly. The flow fundamental equations may be described as follows:

$$\frac{\partial \boldsymbol{\Phi}}{\partial t} + \frac{\partial \boldsymbol{F}_i}{\partial x_i} + \frac{\partial \boldsymbol{G}_i}{\partial x_i} = \boldsymbol{0}, \tag{1}$$

where t denotes time, x_i are the components of the Cartesian coordinates vector, with $i = 1, \ldots, d$, $\boldsymbol{\Phi}$ is the vector of flow conservative variables, $\boldsymbol{F}_i$ and $\boldsymbol{G}_i$ correspond to advective and diffusive terms, respectively, i.e.:

$$\boldsymbol{\Phi} = \begin{Bmatrix} \rho \\ \rho u_j \\ \rho E \end{Bmatrix}, \quad \boldsymbol{F}_i = \begin{Bmatrix} \rho u_i \\ \rho u_j u_i + p\delta_{ji} \\ \rho E + p \;\; u_i \end{Bmatrix}, \quad \boldsymbol{G}_i = \begin{Bmatrix} 0 \\ -\tau_{ji} \\ -\tau_{ij} u_j - k\dfrac{\partial T}{\partial x_i} \end{Bmatrix}, \tag{2}$$

where ρ is the fluid specific mass, u_i are components of the flow velocity vector given according to the Cartesian coordinate directions $i = 1, ..., d$, p is the flow pressure, δ_{ji} are components of the Kronecker's delta, with $j = 1, ..., d$ and $E = e + u_i u_i/2$ is the total energy, with $e = C_v T$ denoting the internal energy, T the absolute temperature, k is the diffusion constant and τ_{ij} are components of the viscous stress tensor [11]. The closure problem associated with Eq. (1) is resolved using the equation of state for perfect gas $p = (\gamma - 1)\rho e$, where $\gamma = C_p/C_v$, with C_p and C_v representing the heat capacity for constant pressure and constant volume, respectively. Boundary and initial conditions must be specified in order to solve the system of flow equations given by Eq. (1). The flow fundamental equations defined in Eq. (1) describe a compressible flow which is numerically solved with a stabilized numerical method, the CBS scheme which can solve a wide range of flow speeds. The equations presented in Eq. (1) are further normalized, being transformed into the non-dimensional Navier-Stokes equations, which are normalized by non-dimensional flow parameters such as the Mach number and Prandlt number. For simulating flows with small compressible effects, a Mach=0.1 flow is considered in the compressible solver, which should reflects non-isothermal incompressible flows. The dimensionless velocity, pressure, energia total e temperatura are given by the relations:

$$\overline{u}_i = \frac{u_i}{u_\infty}, \quad \overline{p} = \frac{p}{\rho_\infty u_\infty^2}, \quad \overline{E} = \frac{E}{u_\infty^2}, \quad \overline{T} = \frac{T c_p}{u_\infty^2}, \tag{3}$$

where an over-bar indicates a non-dimensional quantity and subscript ∞ represents a free stream quantity.
The system of flow equations is discretized here using the Characteristic-Based Split (CBS) scheme [12], where a standard Galerkin weighted-residual procedure is applied in the context of the Finite Element Method (FEM) using linear tetrahedral elements. Considering an explicit scheme, the numerical model utilized here may be expressed with the following algorithm [12]:
- Step 1: solve the first momentum equation to obtain $\boldsymbol{\Delta}\tilde{\boldsymbol{U}}_i^*$:

$$\boldsymbol{M}\boldsymbol{\Delta}\tilde{\boldsymbol{U}}_i^* = \Delta t\Big[\ \boldsymbol{C}-\boldsymbol{S}\quad \tilde{\boldsymbol{u}}_j\tilde{\boldsymbol{U}}_i\ -\ \boldsymbol{K}_\tau-\boldsymbol{T}_\tau\ \ \tau_{ij}\ \Big]^n - \\ -\frac{\Delta t^2}{2}\tilde{\boldsymbol{u}}_k\Big[\ \boldsymbol{K}_u-\boldsymbol{T}_u\quad \tilde{\boldsymbol{u}}_j\tilde{\boldsymbol{U}}_i\ +\ \boldsymbol{K}_p-\boldsymbol{T}_p\ \ \tilde{\boldsymbol{p}}\ \Big]^n; \tag{4}$$

- Step 2: calculate the specific mass increment $\boldsymbol{\Delta}\tilde{\boldsymbol{\rho}}$:

$$\boldsymbol{M}\boldsymbol{\Delta}\tilde{\boldsymbol{\rho}} = \Delta t\Big[\ \boldsymbol{D}-\boldsymbol{R}_u\quad \tilde{\boldsymbol{U}}_i+\theta_1\boldsymbol{\Delta}\tilde{\boldsymbol{U}}_i^*\ -\Delta t\theta_1\boldsymbol{K}\tilde{\boldsymbol{p}}\Big]^n \tag{5}$$

- Step 3: solve the second momentum equation to obtain $\boldsymbol{\Delta}\tilde{\boldsymbol{U}}_i$ and, consequently, U_i^{n+1}:

$$\boldsymbol{M}\boldsymbol{\Delta}\tilde{\boldsymbol{U}}_i = \boldsymbol{M}\boldsymbol{\Delta}\tilde{\boldsymbol{U}}_i^* + \Delta t\Big[\ \boldsymbol{D}-\boldsymbol{R}_u\ \ \tilde{\boldsymbol{p}}\Big]^n \tag{6}$$

- Step 4: solve the energy equation to obtain $\boldsymbol{\Delta}\ \tilde{\boldsymbol{\rho}}\tilde{\boldsymbol{E}}$:

$$\boldsymbol{M}\boldsymbol{\Delta}\ \tilde{\boldsymbol{\rho}}\tilde{\boldsymbol{E}}\ = \Delta t\Bigg[\ \boldsymbol{C}-\boldsymbol{S}\quad \tilde{\boldsymbol{\rho}}\tilde{\boldsymbol{E}}+\tilde{\boldsymbol{p}}\ +\ \boldsymbol{T}_\tau-\boldsymbol{K}_\tau\ \left(k\frac{\partial T}{\partial x_i}+\tau_{ij}\tilde{\boldsymbol{u}}_j\right)\Bigg]^n - \\ -\frac{\Delta t^2}{2}\Big[\tilde{\boldsymbol{u}}_k\ \ \boldsymbol{K}_u-\boldsymbol{T}_u\ \ \tilde{\boldsymbol{u}}_j\ \ \tilde{\boldsymbol{\rho}}\tilde{\boldsymbol{E}}+\tilde{\boldsymbol{p}}\ \Big]^n, \tag{7}$$

where a tilde (~) superscript indicates a nodal value, while the time increment is evaluated considering:

$$\Delta t = \min\left(\frac{l}{\overline{c}+\left|\boldsymbol{u}\right|},\frac{l^2}{2\nu}\right)\theta_c, \tag{8}$$

where θ_c is the constant of Courant-Friedrichs-Lewy, with values specified between 0 and 1, $\overline{c}$ is the local sound speed and l is the element characteristic length. For detailed information on the numerical model utilized in this work, see Linn and Awruch [13].

3 Mesh adaptation

A mesh adaptation scheme based on Riemannian metric is used here to estimate the error and adapt the mesh anisotropically. By employing a Riemannian metric, the error can be estimated directionally as a tensor quantity with a well-established mathematical foundation.

3.1 Metric evaluation

From a discrete point of view, the metric field needs to be interpolated to assess approximate length and size in the Riemannian space. Considering a linear interpolation of the metric tensor, the length $\ell_{\mathcal{M}}(\boldsymbol{ab})$ of an edge $\boldsymbol{ab}$ is obtained as [14]:

$$\ell_{\mathcal{M}}\ \ \boldsymbol{ab}\ \approx \frac{2}{3}\frac{\ell_0^2+\ell_0\ell_1+\ell_1^2}{\ell_0+\ell_1}, \tag{9}$$

where $\ell_i\ \ \boldsymbol{ab}\ = \sqrt{\boldsymbol{ab}^T\mathcal{M}\ \ \boldsymbol{x}_i\ \ \boldsymbol{ab}}$ is the length of an edge $\boldsymbol{ab}$ in the metric system $\mathcal{M}(\boldsymbol{x}_i)$, with $i = 1, 2$ denoting its end points $\boldsymbol{a}$ and $\boldsymbol{b}$. In a similar manner, the volume of an element K in the Riemannian metric space can be numerically approximated as:

$$\left|K\right|_{\mathcal{M}} \approx \sqrt{\det\frac{1}{4}\sum_{i=1}^{4}\mathcal{M}_i\ \ \boldsymbol{x}\ }\ \left|K\right|, \tag{10}$$

where $\mathcal{M}_i(\boldsymbol{x})$ is the metric evaluated at every vertex i of an element K (assumed as a tetrahedral element), while $|K|$ is the volume of the element in the Euclidian metric space.

The anisotropic quality of an element *K* can be monitored through a quality function $Q_{\mathcal{M}}$, which combines information on sizing and orientation [15], i.e.:

$$Q_{\mathcal{M}}\ K\ = \frac{\sum \ell^2_{\mathcal{M}}\ A_K}{\left|K\right|_{\mathcal{M}}}, \tag{10}$$

where A_K are the edges of element K. By minimizing $Q_{\mathcal{M}}$, the element quality is maximized in an anisotropic sense.

The error $\xi(\boldsymbol{ab})$ estimated for an edge $\boldsymbol{ab}$ is defined as the upper limit of the difference between a quadratic approximation and the linear interpolation evaluated for a given continuous function φ, which can be expressed as:

$$\xi\ \boldsymbol{ab}\ \equiv \ell_{\mathcal{M}}\ \boldsymbol{ab}\ , \tag{11}$$

where the metric $\mathcal{M}(\boldsymbol{x})$ is defined as the normalized Hessian of the function φ measured in the norm $\boldsymbol{L}^p$ [16]:

$$\mathcal{M}\ \boldsymbol{x}\ = \mathcal{M}_{\boldsymbol{L}^p}\ \boldsymbol{x}\ =\ \det\left|\boldsymbol{H}\ \varphi\ \right|^{-1/\ 2p+d}\ \left|\boldsymbol{H}\ \varphi\ \right|, \tag{12}$$

where $\boldsymbol{H}(\varphi)$ is a symmetric matrix representing the Hessian of φ. The Hessian matrix is evaluated using a weak formulation based on Green's formula [17].

An element edge $\boldsymbol{ab}$ is refined if $\xi(\boldsymbol{ab}) \geq \eta_U \varepsilon$ and unrefined if $\xi(\boldsymbol{ab}) \leq \eta_L \varepsilon$, where ε is the target adaption error specified by the user. The upper and lower error limit values η_U and η_L are assumed to be 1.4 and 0.6, respectively [14]. In the present investigation, the continuous function φ is associated with the vector of flow variables, that is, $\varphi = [\rho,\ u_1,\ u_2,\ u_3,\ E]$. Metric field intersection are performed in order to evaluate the error associated to the fields $\rho,\ u_1,\ u_2,\ u_3,\ E$ as a minimum intersected field. Node movement is performed moving the nodes along the directions of the edges which they are connected. The movement increases the anisotropic quality of the mesh by minimizing the sum of the quality defined in Eq. 10 for the affected elements. Detailed information on the adaptation scheme utilized in this work may be found in the references [10].

4 Numerical application

Mesh adaptation is adopted here to simulate a tornado-like vortex flow in a cylindrical domain proposed by Nomura et al. [18], which reproduces the geometric configuration similar of the experimental simulator utilized by Matsui and Tamura [19].

The computational domain and boundary conditions utilized in the present investigation are shown in Fig. 1, where linear tetrahedral elements are employed. The mesh adaptation scheme proposed in this work is adopted considering error evaluations based on the flow variables ($\varphi = \rho,\ u_1,\ u_2,\ u_3,\ E$) and a target error $\varepsilon_{\boldsymbol{L}^3} = 0.10$, with error norm $\boldsymbol{L}^3$ and $h_{min} = 0.005$ m.

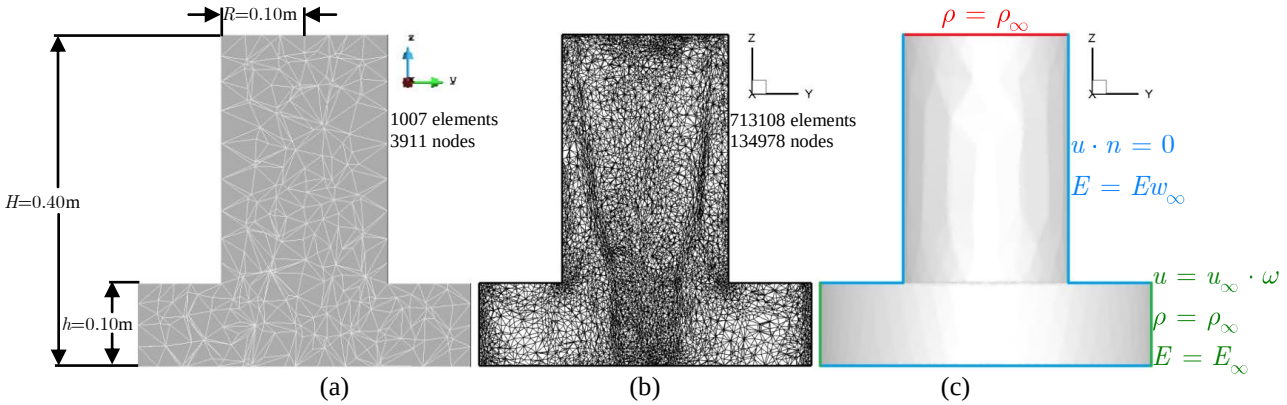

Figure 1. Tornado simulator: (a) computational domain and inicial finite element mesh; (b) adapted finite element mesh; (c) boundary conditions.

Since the boundary conditions proposed by Nomura et al. [18] generate a thermodynamic problem for incompressible flows (the temperature field on the lower cylindrical surface changes to balance the traction-free condition with prescribed angle), the following boundary conditions are utilized (see Fig. 1 (b)): slip conditions

($u \cdot n = 0$) and $E = Ew_\infty$ (total energy is prescribed considering T = 500 ºR = 277.77 K) on the ground and lateral walls (blue lines); $\rho = \rho_\infty$ on the top of the chamber (red line) and $u = u_\infty \cdot \omega$, $\rho = \rho_\infty$ and $E = E_\infty$ on the lateral walls of the lower cylindrical zone (green lines). Flow and computational parameters utilized in the present study are indicated in Tab. 1.

Table 1. Flow and computational parameters.

Variable	Symbol	Value
Reference flow speed (free stream)	u_∞	1.0
Reference specific mass of fluid	ρ_∞	1.0
Inflow direction	ω	37.5°
Swirl ratio	S	0.38
Mach number of the free stream	Ma_∞	0.1
Prandtl number of the free stream	Pr_∞	0.720
Reynolds number of the free stream	Re_∞	450
Courant-Friedrichs-Levy constant	θ_c	0.6

Figure 2 shows the streamlines and the flow velocity field obtained with the numerical model proposed in this work, where dimensionless velocity values $|\boldsymbol{u}|$ are considered. Notice that a typical flow pattern is observed, with helicoidal and ascending streamlines, which correspond to the flow field and velocity values presented by Nomura et al. [18], who identified a maximum dimensionless velocity of $|\boldsymbol{u}|$ = 2.81.

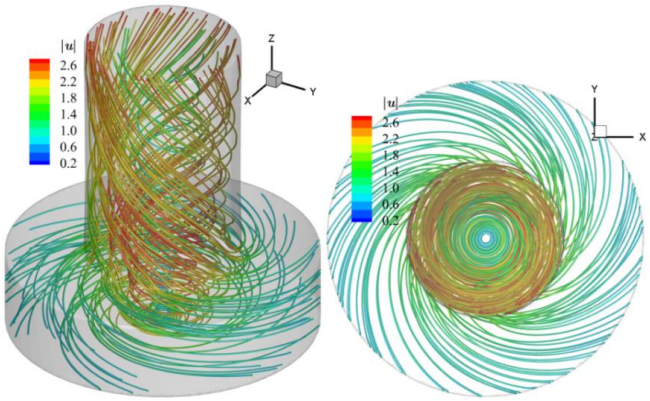

(a) (b)

Figure 2. Streamlines and dimensionless flow velocity field: (a) 3D view; (b) plan view.

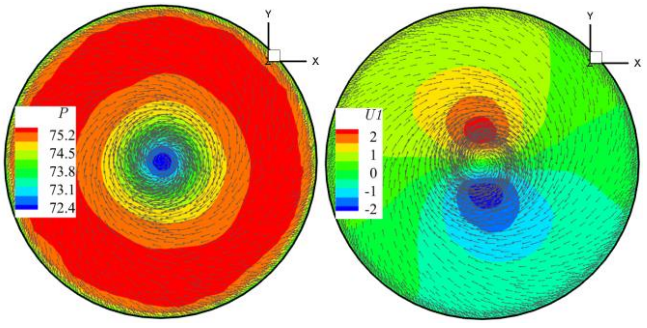

(a) (b)

Figure 3. Flow fields, plan view at $z = x_3 = 0$: (a) dimensionless pressure p; (b) dimensionless flow velocity component u_1.

The dimensionless pressure p and flow velocity component u_1 fields obtained in the present investigation are shown in Fig. 3, where the flow velocity vector field is also presented considering a plan view at $z = x_3 = 0$. One can see that the pressure values indicated here are different from those predicted by Nomura et al. [18], although a decreasing trend for the pressure values can be observed towards the center line of the chamber. The flow velocity component u_1 has maximum values (u_1 = 2.34) at the radial position x_2 = 0.04 m, where the finite element mesh is more dense due to mesh adaptation.

Figure 4 presents plan views at $x = x_1 = 0$ referring to results obtained here for dimensionless pressure, dimensionless flow velocity component u_1 (with the velocity vector field) and temperature (given in Kelvin). The pressure distribution shows the characteristic funnel observed in tornado flow field, with a minimum value p = 70.74 at x_3 = 0.15 m, although a constant pressure profile can be seen at the top of the chamber owing to the boundary conditions utilized in the present investigation. On the other hand, the velocity field presents maximum values at the chamber floor, which is consistent with the boundary condition adopted on that region (slip condition), and decreasing values as the height is increased. The temperature field given in Kelvin shows an approximately uniform distribution with slight decrease with height, where maximum and minimum values are found at the entrance and exit of the computational domain respectively. Notice that the present results can reproduce the vortex breakdown phenomenon (see Fig. 4b), which is characterized by a double circulation zone near the top of the experimental simulator [19]. This flow pattern was not observed in Nomura et al. [18].

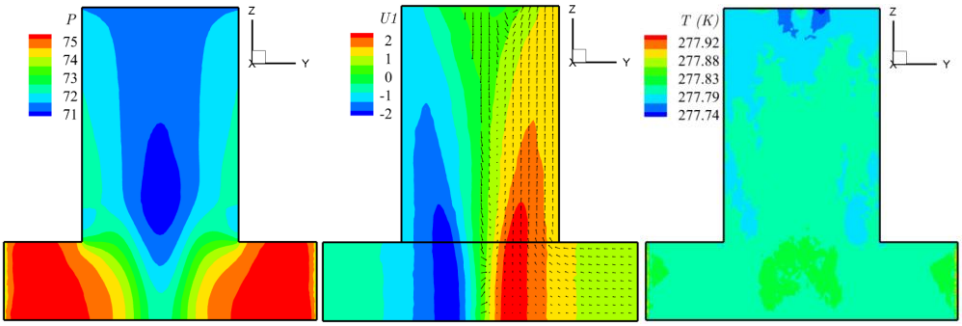

(a) (b) (c)

Figure 4. Flow fields, plan view at $x = x_1 = 0$: (a) dimensionless pressure p; (b) dimensionless velocity component u_1; (c) temperature T [Kelvin].

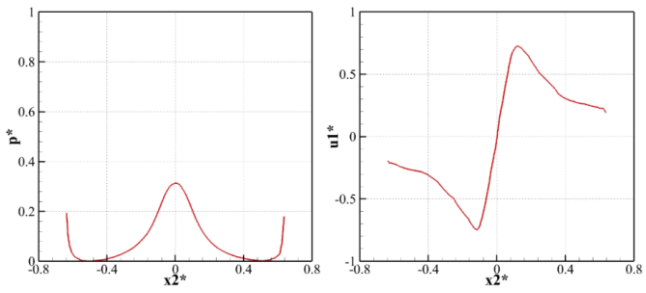

(a) (b)

Figure 5. Pressure and velocity profiles at $x_1 = x_3 = 0$: (a) modified pressure p*; (b) dimensionless velocity u_1*.

In Fig. 5, distributions of modified pressure $p^* = p - 75.3847 \ / \ 1.0 \cdot 3.1734^2$ and dimensionless flow velocity $u_1^* = u_1 \ / \ 3.1734$ are presented along the dimensionless radial coordinate $x_2^* = x_2 h \ / \ \pi R^2$. It is observed that the maximum value of modified pressure (p* = 0.31) is 43% lower than that obtained by Nomura et al. [18], although the pressure profile shows a similar shape, with exception of extreme x_2* values, where the pressure values presented a different behavior owing to the boundary conditions adopted here with respect to total energy E. The dimensionless velocity profile obtained here corresponds to the distribution presented by Nomura et al. [18], but the maximum values (u_1* = 0.74) are 23% higher than that obtained by the reference

work. It is important to notice that Nomura et al. [19] utilized a coarse mesh, with no adaptation scheme, and a lower swirl ration ($S = R\tan\omega \,/\, 2h$) than that obtained here ($S \approx 1.50$ with $\omega \approx 71.6$).

5 Conclusions

A numerical model based on the explicit Characteristic-Based Split (CBS) scheme was proposed in this work for tornado flow simulation, where Adaptive Mesh Refinement (AMR) techniques were utilized. A characteristic tornado chamber was numerically simulated and results demonstrated that the adaptation scheme adopted here was able to reproduce typical flow patterns observed in tornado vortex flows. In future research the fluid flow should be considered as transient and a larger Re number should be investigated, where turbulent effects would be present.

Acknowledgements. The authors would like to thank the National Council for Scientific and Technological Development (CNPq, Brazil) for the financial support.

Authorship statement. The authors hereby confirm that they are the sole liable persons responsible for the authorship of this work, and that all material that has been herein included as part of the present paper is either the property (and authorship) of the authors, or has the permission of the owners to be included here.

References

[1] H. E. Brooks, J. W. Lee, and J. P. Craven, "The spatial distribution of severe thunderstorm and tornado environments from global reanalysis data," *Atmos. Res.*, vol. 67–68, pp. 73–94, 2003.
[2] M. A. F. Silva Dias, "An Increase in the Number of Tornado Reports in Brazil," *Weather. Clim. Soc.*, vol. 3, no. 3, pp. 209–217, 2011.
[3] N. B. Ward, "The Exploration of Certain Features of Tornado Dynamics Using a Laboratory Model," *J. Atmos. Sci.*, vol. 29, no. 6, pp. 1194–1204, 1972.
[4] F. L. Haan Jr., P. P. Sarkar, and W. A. Gallus, "Design , construction and performance of a large tornado simulator for wind engineering applications," vol. 30, pp. 1146–1159, 2008.
[5] A. R. Mishra, D. L. James, and C. W. Letchford, "Physical simulation of a single-celled tornado-like vortex , Part A : Flow field characterization," *J. Wind Eng. Ind. Aerodyn.*, vol. 96, pp. 1243–1257, 2008.
[6] M. Refan, "Physical Simulation of Tornado-Like Vortices," The University of Western Ontario, 2014.
[7] D. S. Nolan, A. S. Almgren, and J. B. Bell, "High Reynolds Number Simulations of Axisymmetric Tornado-like Vortices with High Reynolds Number Simulations of Axisymmetric Tornado-like Vortices with Adaptive Mesh Refinement," Berkeley, CA, 1999.
[8] D. S. Nolan, A. S. Almgren, and J. B. Bell, "Studies of the Relationship Between Environmental Forcing and the Structure and Dynamics of Tornado-like Vortices," Berkeley, California, 2000.
[9] D. Natarajan, "Numerical Simulation of Tornado-like Vortices," The University of Western Ontario, 2011.
[10] R. V. Linn, "Simulação de Escoamentos Compressíveis Turbulentos no Entorno de Corpos Móveis Usando Malhas Adaptativas de Elementos Finitos," Universidade Federal do Rio Grande do Sul, 2017.
[11] H. (Deceased) Schlichting and K. Gersten, *Boundary- Layer Theory*, 9th ed. Berlin Heidelberg: Springer, Berlin, Heidelberg, 2017.
[12] O. C. Zienkiewicz, R. L. Taylor, and P. Nithiarasu, *The Finite Element Method for Fluid Dynamics*, Seventh. Kidlington, Oxford: Butterworth-Heinemann, Elsevier, 2014.
[13] R. V. Linn and A. M. Awruch, "Unstructured Anisotropic Mesh Adaptation for Compressible Flows using Refinement and Coarsening Procedures," in *Mecánica Computacional*, 2013, vol. XXXII, pp. 1213–1237.
[14] W. G. Habashi, J. Dompierre, Y. Bourgault, D. Ait-Ali-Yahia, M. Fortin, and M.-G. Vallet, "Anisotropic mesh adaptation : towards user-independent , Part I : general principles," *Int. J. Numer. Methods Fluids*, vol. 32, no. 6, pp. 725–744, 2000.
[15] V. Ducrot, P. Frey, and A. Claisse, "Levelsets and anisotropic mesh adaptation," *Am. Inst. Math. Sci.*, vol. 23, no. 1&2, pp. 165–183, 2009.
[16] A. Loseille and F. Alauzet, "Continuous Mesh Framework Part I: Well-Posed Continuous Interpolation Error," *SIAM J. Numer. Anal.*, vol. 49, no. 1, pp. 38–60, 2011.
[17] M.-G. Vallet, C.-M. Manole, J. Dompierre, S. Dufour, and F. Guibault, "Numerical comparison of some Hessian recovery techniques," *Int. J. Numer. Methods Eng.*, vol. 72, no. 8, pp. 987–1007, 2007.
[18] T. Nomura, S. Miyata, and H. Hasebe, "AN ATTEMPT OF FINITE ELEMENT FLOW SIMULATION OF TORNADO VORTICES," in *The Seventh Asia-Pacific Conference on Wind Engineering*, 2009, p. 8.
[19] M. Matsui and Y. Tamura, "Influence of swirl ratio and incident flow conditions on generation of tornado-like vortex,"